Letter

Energies and spectra of solids from the algorithmic inversion of dynamical Hubbard functionals

Tommaso Chiarotti [1,*] Andrea Ferretti [2] and Nicola Marzari [1,3]

[1]*Theory and Simulations of Materials (THEOS) and National Centre for Computational Design and Discovery of Novel Materials (MARVEL), École Polytechnique Fédérale de Lausanne, 1015 Lausanne, Switzerland*

[2]*Centro S3, CNR–Istituto Nanoscienze, 41125 Modena, Italy*

[3]*Laboratory for Materials Simulations (LMS), Paul Scherrer Institut (PSI), 5232 Villigen PSI, Switzerland*

(Received 25 February 2023; revised 16 November 2023; accepted 22 May 2024; published 29 July 2024)

Energy functionals of the Green's function can simultaneously provide spectral and thermodynamic properties of interacting electrons' systems. Although powerful in principle, these formulations need to deal with dynamical (frequency-dependent) quantities, increasing the algorithmic and numerical complexity and limiting applications. We first show that, when representing all frequency-dependent propagators as sums over poles—a truncated Lehmann representation—, the typical operations of dynamical formulations become closed (i.e., all quantities are expressed as sums over poles) and analytical. In the framework, the Dyson equation is mapped into a nonlinear eigenvalue problem that can be solved exactly; this is achieved by introducing a fictitious noninteracting system with additional degrees of freedom, which shares, upon projection, the same Green's function of the real system. In addition, we introduce an approximation to the exchange-correlation part of the Klein functional adopting a localized *GW* approach; this is a generalization of the static Hubbard extension of density-functional theory with a dynamical screened potential $U(\omega)$. We showcase the algorithmic efficiency of the method, and the physical accuracy of the functional, by computing the spectral, thermodynamic, and vibrational properties of $SrVO_3$, finding results in close agreement with experiments and state-of-the-art methods, at highly reduced computational costs and with a transparent physical interpretation.

DOI: 10.1103/PhysRevResearch.6.L032023

Accurate and predictive first-principles calculations of materials properties have been and remain a challenging task for scientific discoveries and technological innovation [1]. Although density-functional theory (DFT) has provided a major step forward in the prediction of ground-state properties [2,3], addressing spectroscopic quantities remains challenging [4–7]. To overcome this limitation, dynamical methods, mostly based on Green's functions, have been used; these include many-body perturbation theory (MBPT) approaches such as *GW* [5,8], dynamical mean-field theory [7,9] (DMFT), spectral functional theories [6,10,11] (SFT), and electron-boson interaction schemes [12–14]; in all of these approaches, dynamical (frequency-dependent) self-energies or potentials arise.

In Green's function theories, the Luttinger-Ward (LW) and Klein functionals [15–19] are energy functionals of the Green's function that are variational and yield conserving potentials that are dynamical. Although explicitly known diagrammatically, the exact exchange-correlation term Φ_{xc} of the functional is computationally inaccessible and needs to be approximated [20,21]. The choice of the approximation for Φ_{xc} determines the physics accessible to the functional, ranging from long-range plasmonic effects, as in *GW* [5,8], to strong correlations as in DMFT [7,9]. The stationarity condition of the functional yields the Dyson equation involving the interacting propagator G and the dynamical self-energy (as a derivative of Φ_{xc} with respect to G) [18,19]. Therefore, the functional and its derivative determine the thermodynamics and the spectral properties of a material, also allowing one to compute, at self-consistency, ground-state quantities such as forces and phonons through the Hellmann-Feynman theorem [22].

Due to the presence of dynamical quantities, applications where both spectroscopic and thermodynamic quantities are computed together are limited (see Ref. [23] and references therein). In the context of *GW*, such calculations have been performed for model systems, such as the homogeneous electron gas [24] or Hubbard chains [25–27], and later extended to solids, typically using an imaginary-axis formalism [28–31]. This latter approach has been proven very effective for the prediction of ground-state properties but retains limited accuracy for spectral properties, due to the challenges of performing the analytic continuation to the real axis [32]. Similarly, in DMFT, it is possible to calculate different ground-state properties accurately [33,34], while spectral properties still need to deal with analytic continuation.

In this letter, we propose a framework to enable the calculation of accurate spectral and thermodynamic properties on the same footing, and apply it to study $SrVO_3$. First, we generalize to the nonhomogeneous case the algorithmic-inversion method on sum over poles (AIM-SOP) [23] to tackle dynamical formulations (e.g., MBPT or DMFT) for condensed-matter

*Contact author: tommaso.chiarotti@epfl.ch

applications; here, the dynamical (frequency-dependent) propagators are represented as sum over poles (SOP) and defined on the entire complex plane, thus avoiding analytic continuation (for clarity, by SOP we imply a sum over first-order poles). Second, we introduce a dynamical Hubbard functional that generalizes the DFT+U energy functional of Dudarev *et al.* [35] to host a dynamical screened potential $U(\omega)$, rather than a static U, and that can be applied to solids with localized d or f frontier electrons. Third, we use AIM-SOP to implement the dynamical Hubbard functional and obtain the spectral and thermodynamic properties of $SrVO_3$, a paradigmatic correlated metal. We find very good agreement with experiments and state-of-the-art methods, such as GW+DMFT, for the spectrum, bulk modulus, and phonons, at a greatly reduced computational cost compared to established approaches.

Algorithmic-inversion method on sum over poles. AIM-SOP provides a theoretical and computational framework aimed to deal with dynamical quantities, such as Green's functions (GF) and self-energies (SE), and which is closed for common operations appearing in many-body perturbation theory (MBPT), i.e., all quantities are expressed as sums over poles. Starting from our previous study [23], here we generalize the framework to the operatorial case to address realistic materials. AIM-SOP is based on the representation of dynamical (frequency-dependent) propagators as sum over poles,

$$\Sigma(\mathbf{r},\mathbf{r}',\omega)=\sum_{i=1}^{N}\frac{\Gamma_i(\mathbf{r},\mathbf{r}')}{\omega-\Omega_i}+\Sigma_0(\mathbf{r},\mathbf{r}'), \tag{1}$$

where Σ may be a generic propagator (not only a SE, but also, e.g., the GF or the polarizability), Γ_i are operatorial residues (we omit spacial and orbital indexes henceforth), Ω_i are scalar poles, and Σ_0 is a static operator (for example, the Hartree-Fock term). In general, all time-ordered (TO) operators can be expanded as SOP [36]. It is evident that the sum of two operators on SOP is a SOP, and the same holds for multiplication and convolutions [23]. In addition, and crucially, the Dyson equation $G(\omega)=[\omega I-h_0-\Sigma(\omega)]^{-1}$ is closed on SOP, i.e., a self-energy on SOP yields a GF on SOP.

To demonstrate this, we start by observing that the frequency-wise inversion of the Dyson equation can be exactly mapped into the solution of the nonlinear eigenvalue problem,

$$[h_0+\Sigma(\omega)]|\psi\rangle=\omega|\psi\rangle, \tag{2}$$

where the nonlinear eigenvalues are the poles of the Green's function and the eigenvectors determine its residues. In fact, as derived in the Supplemental Material [37] (and in Ref. [38] within the mathematical framework of NLEPs), if the self-energy can be represented as a sum over poles (i.e., it is rational on the whole complex plane), the resulting GF is also a SOP,

$$G(\omega)=\sum_s\frac{|\psi_s^r\rangle\langle\psi_s^l|}{\omega-z_s}, \tag{3}$$

where (z_s,ψ_s^r) are the nonlinear eigenvalues and (right) eigenvectors of Eq. (2). Of course, when dealing with the exact self-energy, the Lehmann representation of the Green's function guarantees Eq. (3), but the extension to approximate self-energies requires the mathematical treatment of NLEPs [37,38]. Moreover, in writing Eq. (3) we have assumed the completeness of the nonlinear left/right eigenvectors; we also mention that, in the more general case of a self-energy that is analytic in a connected set of the complex plane, one needs to add to the rhs of Eq. (3) an analytic remainder function—see Supplemental Material [37] for an in-dept discussion.

Although there are multiple ways to solve Eq. (2) (e.g., see Refs. [38] or [39]), here we exploit the knowledge of residues and poles of the SE in Eq. (1) to find the SOP for the GF. Introducing a factorization of the self-energy residues $\Gamma_m=V_m\bar{V}_m^\dagger$ in Eq. (1), the Dyson equation can be rewritten as

$$G(\omega)=\left[\omega I-h_0-\sum_{m=1}^{N}V_m(\omega-\Omega_m)^{-1}\bar{V}_m^\dagger\right]^{-1}. \tag{4}$$

This can be interpreted as embedding a noninteracting system h_0 with N noninteracting fictitious degrees of freedom, representing the bath, each having a Hamiltonian Ω_m [40] coupled to h_0 by V_m and $\bar{V}_m^\dagger$. As can be proven by a direct calculation, the Green's function in Eq. (4) can be obtained as $G(\omega)=P_0(\omega I_{\rm tot}-H_{\rm AIM})^{-1}P_0$ and

$$H_{\rm AIM}=\begin{pmatrix} h_0 & V_1 & \dots & V_N \\ \bar{V}_1^\dagger & \Omega_1 I_1 & 0 & 0 \\ \vdots & 0 & \ddots & 0 \\ \bar{V}_N^\dagger & 0 & \dots & \Omega_N I_N \end{pmatrix}, \tag{5}$$

with P_0 projecting onto the h_0 Hilbert space. We carry out the proof by exploiting embedding techniques in the Supplemental Material [37]. To summarize, AIM-SOP exactly maps the nonlinear eigenvalue problem, Eq. (2), into a linear eigenvalue problem by building a fictitious noninteracting system, with additional degrees of freedom (DOFs), that possesses the same GF as the interacting system upon projection. As a side but important note, the freedom in the factorization of Γ_m can be exploited to minimize the dimension of the bath. In fact, when using SVD to factorize Γ_m, the number of columns (rows) of V_m ($\bar{V}_m^\dagger$) is reduced to the rank of Γ_m, thus making $\dim[I_m]=\mathrm{rank}[\Gamma_m]$. Then, the dimension of $H_{\rm AIM}$ is reduced to $\dim[H_{\rm AIM}]=\dim[h_0]+\sum_m\mathrm{rank}[\Gamma_m]$.

It is important to note that, at variance with our previous study [23], in Eq. (5) the entries are matrix blocks and not scalars, also making apparent the link to NLEPs. In mathematical terms this treatment can be seen as a special case of the "linearization" of NLEPs using rational functions [38], with the $H_{\rm AIM}$ matrix serving as an *ad hoc* alternative to the companion matrix or other approaches [39]. In electronic-structure methods, a construction comparable to $H_{\rm AIM}$ is used in the context of DMFT to efficiently invert the Dyson equation [7,41]. Here, also owing to the connection to the NLEP framework, the case of fully non-Hermitian (diagonalizable) Hamiltonians is also included, e.g., with $V_m\neq\bar{V}_m$ and complex Ω_m. In the Supplemental Material [37] we also discuss the case of nondiagonalizable Hamiltonians together with the appearance of higher-order poles in the solution of the Dyson equation. By linking this approach to the theory of embedding and unfolding, it becomes apparent that the methods in Refs. [42–45], all involving the construction of a supermatrix (or upfolded matrix) to solve the Dyson equation for the self-energy or the Bethe-Salpeter equation, can be seen as specialized cases of the present framework. It is important to stress that to maintain

computational efficiency it is essential to have a SOP representation of the self-energy; so, the physical and algorithmic assumption here is to work with approximate but analytical propagators (as SOP), and to solve exactly the Dyson equation within this representation. In addition, in Ref. [46] we complement the approach with the AIM-SOP reversed, i.e., from the SOP of the GF we obtain the SOP of the SE.

Dynamical Hubbard functional. Taking AIM-SOP as a formal and effective approach to solving electronic-structure problems subject to dynamical potentials, we introduce a functional formulation that extends the DFT+U energy functional of Dudarev *et al.* [35] to host a frequency-dependent screened potential $U(\omega)$. In particular, we define a "dynamical Hubbard" Klein energy functional as

$$E_{\rm dynH}[G] = E_H[\rho] + E_{xc}[\rho] + \Phi_{\rm dynH}[\mathbf{G}] - {\rm Tr}_\omega\left[G_0^{-1}G\right] + {\rm Tr}_\omega {\rm Log}\, G_0^{-1}G + {\rm Tr}_\omega[h_0 G_0]. \quad (6)$$

Here, ${\rm Tr}_\omega[...]$ stands for $\int \frac{d\omega}{2\pi i} e^{i\omega 0^+} {\rm Tr}[...]$, G represents the Green's function (GF) of the system, $G_0^{-1} = \omega I - h_0$ is the Kohn-Sham Green's function, ρ is the density derived from G, and $\mathbf{G}$ is the projection of G onto a localized manifold (typically d or f states), commonly referred to as the Hubbard manifold. For a single site, this dynamical Hubbard energy correction reads

$$\Phi_{\rm dynH}[\mathbf{G}] = \frac{1}{2}\int \frac{d\omega}{2\pi i}\frac{d\omega'}{2\pi i} e^{i\omega 0^+} e^{i\omega' 0^+} U(\omega') \times {\rm Tr}\{\mathbf{G}(\omega+\omega')[\delta(\omega - c)\mathbf{I} - \mathbf{G}(\omega)]\}, \quad (7)$$

where $U(\omega)$ represents the screened potential $W(\omega)$ of the system projected onto a localized (Hubbard) space and averaged over it, and c is a constant to fix double counting (DC). The DC term is included because we are correcting an approximate DFT functional, and its purpose is to suppress the exchange-correlation interactions of the localized manifold included at the DFT level (for a comprehensive review, see e.g., Ref. [47]).

To justify the ansatz for $\Phi_{\rm dynH}[\mathbf{G}]$, we first look at its derivative, i.e., the (time-ordered) self-energy,

$$\mathbf{\Sigma}_{\rm dynH}(\omega) = 2\pi i \frac{\delta \Phi_{\rm dynH}[\mathbf{G}]}{\delta \mathbf{G}} = -\int \frac{d\omega'}{2\pi i} e^{i\omega' 0^+} U(\omega')\mathbf{G}(\omega+\omega') + \frac{1}{2}U(c)\mathbf{I}, \quad (8)$$

which is composed of a localization of the *GW* SE [48,49] (first term), and the double-counting term $\frac{1}{2}U(c)\mathbf{I}$. In particular, as shown in Sec. S5 of the Supplemental Material [37] and similarly in Ref. [49], the dynamical Hubbard self-energy can be derived from the *GW* self-energy by discarding the itinerant part of the Lehmann (or KS) amplitudes. Also, if a static screening is considered, $\Phi_{\rm dynH}$ reduces to the (static, rotationally invariant) DFT+U Hubbard correction of Ref. [35]. Indeed, similar to considering DFT+U a truncation of COHSEX [50], the dynamical Hubbard functional stems from a localization of *GW* [49]. Note that, at variance with Ref. [49], the SE of Eq. (8) preserves the correct time ordering, as no approximation in the frequency convolutions was carried out. Additionally, $\Phi_{\rm dynH}$ reduces to the GW_0 functional (plus a double-counting term) in the limit of the Hubbard manifold becoming the entire space. The generalization to multiple sites consists of summing different Φ^I terms, one per site, and is not treated here for simplicity. Note that, as discussed in Sec. S6 of the Supplemental Material [37], we fix the double counting parameter c as $c \to \infty$, so that $U(c) = U_\infty$, i.e., the bare Coulomb potential localized and averaged on the manifold.

Being a Klein functional with the screened interaction set to $U(\omega)$, $E_{\rm dynH}[G]$ can be made stationary by solving self-consistently the corresponding Dyson equation with a static term $h_0 = h_{\rm KS}(\rho)$ and a SE, $\Sigma_{\rm dynH}(\omega) = \sum_{m,m'} |\phi_m\rangle \mathbf{\Sigma}^{mm'}_{\rm dynH}(\omega)\langle\phi_{m'}|$, where $\{\phi_m\}$ span the localized Hubbard manifold for each unit cell (summation over Bravais vectors is left implicit, see note [51]). Here, the use of the algorithmic inversion method is crucial and provides a closed (all within SOPs) formulation. This means that given an initial GF expressed as SOP, e.g., $G = G_{\rm KS}$, and a SOP for the screened interaction $U(\omega)$, the SE $\Sigma_{\rm dynH}$ can also be written as a SOP. Indeed, as mentioned above, the convolution of two SOPs is a SOP [23], and the projections are just linear operations on the residues.

With a SE on SOP, the algorithmic inversion method can be used to find the SOP for the GF. The cycle can then be iterated until self-consistency. Furthermore, the SOP form of the Green's function naturally allows for the accurate evaluation of the generalized Hubbard energy of Eq. (7), the chemical potential, and, in general, integrated thermodynamic quantities [23]. In Ref. [48] Miyake *et al.* observe that their version of localized GW, termed G_dW—same as Eq. (8) but with a different choice of double counting, see Supplemental Material [37]—gives very similar spectral results when the full $\mathbf{k}$-dependent *GW* self-energy is localized onto the manifold. Here, similarly to G_dW [48], we first localize and then calculate the self-energy, given the existence of an energy functional for this form and the link to DFT+U.

Application to $SrVO_3$. As a case study, we apply the formalism to $SrVO_3$. This material is prototypical since it possesses localized electrons around the Fermi energy with d character that are not strongly correlated [53,54], and can thus be described within a *GW*-like approximation. Furthermore, localized *GW* has shown to provide qualitatively good spectral results for this material [48] by improving the *GW* bandwidth [48,53] and yielding results similar to *GW* + EDMFT [54]. Here, we take a step further and compute not only the spectral properties of the material but also integrated quantities, such as the total energy and its derivatives (lattice parameter, bulk modulus, phonons), obtained from the functional $E_{\rm dynH}[G]$. Note that, while we choose to study a metallic system, the framework can be readily applied to semiconductors and insulators. As mentioned, a choice of $U(\omega)$, accounting for the dynamical screening of the electrons in the Hubbard localized manifold is needed. We consider $U(\omega)$ to be the average over the Hubbard manifold of the screened interaction W in the random-phase approximation (RPA); at variance with EDMFT, which uses a cRPA screening [54–56], here we retain screening originating from all the bands (see the Supplemental Material [37] and the references therein for a discussion).

Although designed for self-consistency, here we limit the approach to a one-shot calculation—i.e., a single step in the stationarization of $E_{\rm dynH}$—using as a starting propagator

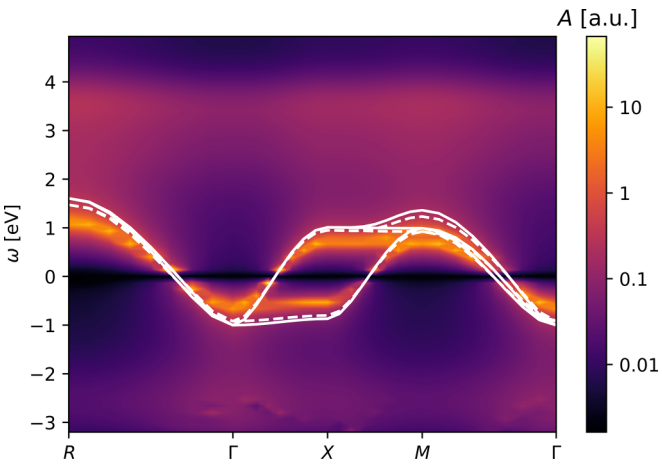

FIG. 1. Spectral function [52] of $SrVO_3$ from this work (color plot) compared to PBEsol (solid-white line) and PBEsol+U (dashed-white line). Only the t_{2g} bands are displayed. The chemical potential is shifted to 0 in all three cases. The color map is logarithmic.

the self-consistent Kohn-Sham Green's function computed with a standard semilocal DFT exchange-correlation functional (PBEsol [57,58]). By doing so, we need to evaluate the energy functional at $E_{\text{dynH}}[G = G_{\text{KS}}]$, and the same for the self-energy, $\Sigma_{\text{dynH}}[\mathbf{G} = \mathbf{G}_{\text{KS}}]$. Then, exploiting the algorithmic inversion method, we find the resulting non-self-consistent Green's function. At this level, the dynamical Hubbard Klein energy functional simplifies to

$$E_{\text{dynH}}[G_{\text{KS}}] = E_{\text{DFT}}[\rho] + \Phi_{\text{dynH}}[\mathbf{G}_{\text{KS}}], \tag{9}$$

correcting the DFT energy with a dynamical energy term. In this letter, we use this last equation to evaluate the energy, and give all the numerical details of the simulations in the Supplemental Material [37]. To go beyond such approximation, please refer to Ref. [46], where we use AIM-SOP to obtain an expression for $\text{Tr}_\omega \text{Ln}\{G_0^{-1} G\}$ in terms of the SOP of the Green's function and self-energy.

In Fig. 1 we present the spectral function resulting from our calculations. In contrast to DFT (PBEsol) or DFT+U (PBEsol+U), which only shift the chemical potential, the spectral function derived from Σ_{dynH} drives a reduction in the bandwidth, along with a renormalization of the full width of the t_{2g} bands. Table I provides details on the bandwidth (BW), the mass enhancement factor (m^*/m_{PBEsol}), and the positions of the lower/upper satellites (LS/US) plus/minus the broadening. While PBEsol and PBEsol+U overestimate both the occupied and full bandwidth, the present results align well with the data from Ref. [48], obtained through localized-*GW* calculations (referred to as qp-locGW in the Table, as only the quasiparticle band structure is computed), and also closely match experimental data [61,62] and results from DMFT [54,59,60].

Compared to the *GW* calculations in Ref. [53], the present results provide a further reduction in the bandwidth, from approximately 0.65 eV to about 0.5 eV. An asymmetric renormalization of t_{2g} with respect to the Fermi energy, absent in the *GW* calculations, is also observed. Naturally, these effects are due to the localized nature of the correction. Concerning the satellites, the LS position is slightly underestimated (i.e., deeper in energy) compared to DMFT and *GW*, but exhibits a significant broadening of around 1 eV, making it still consistent with the references. While the position of the first upper satellite (US1) agrees with *GW* + EDMFT and *GW* + C results, the appearance of a second upper satellite (US2) at about 3.5 eV (similarly to *GW*) differs. A more detailed discussion of the incoherent part of the spectrum, density of states, and self-energy can be found in the Supplemental Material [37]. Notably, the consistency of the quasiparticle results across different choices for the double-counting terms (this letter and Ref. [48]) is reassuring. Additionally, the use of ortho-atomic *d* orbitals to define the localized manifold, instead of maximally localized Wannier functions from the dp model as done in Ref. [48], confirms that results are robust against specific details of the localized *d* manifold for this material. However, this may not always be the case, as, for instance, in situations where Wannier functions hybridize or localize along bonds.

TABLE I. Occupied bandwidth (BW) of the t_{2g} bands, the mass enhancement factor (m^*/m_{PBEsol}), and energy of the lower (LS) and upper satellites (US) from experiments and different theoretical frameworks—with two numbers indicating two different satellites. Results from the generalized dynamical Hubbard functional introduced in this work are estimated from the spectral function in Fig. 1. m^*/m_{PBEsol} is estimated using the ratio of the full bandwidths (LDA and PBEsol coincide). All energies are in eV.

Method	BW	m^*/m_{PBEsol}	LS	US
PBEsol	1.0	1		
PBEsol+U	0.92	1.1		
GW [53]	0.65	1.5	−2	2.2 3.5
GW+C [53]	0.65	1.5	−2	2.2
(qp)locGW [48]	0.5	2		
GW+DMFT [59]	0.5	2	−1.6	2
GW+DMFT [60]	0.6	2	−1.5	2.5
GW+EDMFT [54]			−1.7	2.8
This work	0.5	2	-2.5 ± 1	$\begin{matrix}2.6\\3.5\end{matrix} \pm 1$
Exp. [61]	0.7	1.8	−1.5	
Exp. [62]	0.44	2	−1.5	

From the knowledge of the SOP of the Green's function (here KS) and the functional form of Φ_{dynH}, one can straightforwardly calculate total energies and total-energy differences. In Fig. 2 we compare the equation of state for $SrVO_3$ obtained from PBEsol, PBEsol+U, and the present dynamical formulation. In the legend, we report the estimated values for the equilibrium volume *V* and the bulk modulus *B*, using a Birch-Murnaghan third-order function for the fitting [64]. It can be observed that the present approach correctly predicts the softening of the bulk modulus while overcorrecting the equilibrium lattice parameter. Furthermore, in the Supplemental Material [37] we link the softening of the bulk modulus to the change of the charge density from the different approaches. While these findings are encouraging, they are to be considered preliminary in view of the absence of self-consistency.

Finally, utilizing the relaxed structures and capitalizing on the cost effectiveness of the present method,

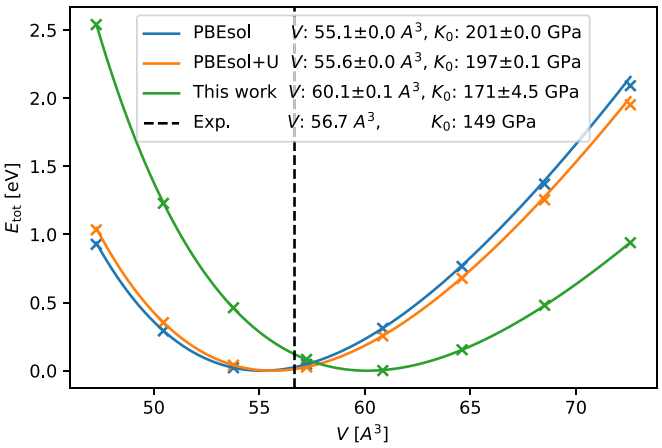

FIG. 2. Equation of state for $SrVO_3$ calculated using PBEsol (blue), PBEsol+U (orange), and the present approach (green). Data (crosses) are fitted using the Birch-Murnaghan curve (solid line). The values and errors obtained using the fit are displayed in the legend. For reference, the experimental volume is marked in dashed black, and the bulk modulus is reported in the legend. Experimental values are taken from [63].

we compute the zone-center phonons for $SrVO_3$. Data are reported in Table II. Since, given the lack of self-consistency, the Hellmann-Feynman theorem does not apply, we use finite-energy differences. Consistent with the softening of the bulk modulus, the first two frequencies are lower compared to PBEsol calculations. Additionally, similar to state-of-the-art methods such as LDA+EDMFT [34], the remaining optical modes are shifted to higher frequencies.

In conclusion, in this letter, we provide a computationally straightforward Green's function framework to address the electronic structure of materials exhibiting correlation in a localized manifold. First, we establish a connection between the solution of the Dyson equation and nonlinear eigenvalue problems; then we solve the equation exactly by extending the algorithmic inversion method on sum over poles (AIM-SOP), introduced in Ref. [23], to the general nonhomogeneous (matricial) case to treat realistic materials. Next, we present an approximation to the exchange-correlation Φ_{xc}

TABLE II. Zone center phonons for $SrVO_3$ calculated with different approaches; the last column shows the results obtained using the generalized dynamical functional introduced in this letter (on top of PBEsol). The data from Ref. [34] have been estimated from the plot. Frequencies are in terahertz.

(THz)	PBEsol	LDA+EDMFT [34]	This work
ω_1	4.86	4.3	3.9
ω_2	10.3	9.0	9.4
ω_3	11.0	11.2	12.1
ω_4	17.3	18.9	19.4

part of the Klein energy functional, yielding a localized-*GW* self-energy, and providing a dynamical generalization of DFT+U. We combine this functional with the algorithmic inversion method to study the paradigmatic case of $SrVO_3$. Our results closely agree with state-of-the-art computational approaches but come with a very modest computational cost. The method allows one to simultaneously access spectral and thermodynamic properties, including total energies and their differences. Moreover, the existence of a Klein functional guarantees the possibility of performing self-consistent calculations. This, in turn, will enable the use of the Hellmann-Feynman theorem to calculate forces and other derivatives within a Green's function formalism. Additionally, besides self-consistency, the method is readily applicable to the study of insulating materials. For example, it can be used to correct erroneous metallic ground states predicted by semilocal DFT, as is often the case with DFT+U. For a detailed discussion of the topics of this letter please also refer to T.C. Ph.D. Thesis [65].

We acknowledge stimulating discussions with M. Caserta and M. Vanzini. This work was supported by the Swiss National Science Foundation (SNSF) through Grant No. 200020_213082 (T.C.) and NCCR MARVEL (N.M.), a National Centre of Competence in Research through Grant No. 205602, and from the EU Commission for the MaX Centre of Excellence on Materials Design at the eXascale under Grant No. 101093374 (A.F.).

[1] N. Marzari, A. Ferretti, and C. Wolverton, Electronic-structure methods for materials design, Nat. Mater. **20**, 736 (2021).
[2] P. Hohenberg and W. Kohn, Inhomogeneous electron gas, Phys. Rev. **136**, B864 (1964).
[3] W. Kohn and L. J. Sham, Self-consistent equations including exchange and correlation effects, Phys. Rev. **140**, A1133 (1965).
[4] J. P. Perdew, W. Yang, K. Burke, Z. Yang, E. K. U. Gross, M. Scheffler, G. E. Scuseria, T. M. Henderson, I. Y. Zhang, A. Ruzsinszky *et al.*, Understanding band gaps of solids in generalized Kohn-Sham theory, Proc. Natl. Acad. Sci. USA **114**, 2801 (2017).
[5] L. Reining, The GW approximation: Content, successes and limitations, Wiley Interdiscip. Rev. Comput. Mol. Sci. **8**, e1344 (2018).
[6] A. Ferretti, I. Dabo, M. Cococcioni, and N. Marzari, Bridging density-functional and many-body Perturbation theory: Orbital-density dependence in electronic-structure functionals, Phys. Rev. B **89**, 195134 (2014).
[7] G. Kotliar, S. Y. Savrasov, K. Haule, V. S. Oudovenko, O. Parcollet, and C. A. Marianetti, Electronic structure calculations with dynamical mean-field theory, Rev. Mod. Phys. **78**, 865 (2006).
[8] L. Hedin and S. Lundqvist, Effects of electron-electron and electron-phonon interactions on the one-electron states of solids, in *Solid State Physics*, Vol. 23, edited by F. Seitz, D. Turnbull, and H. Ehrenreich (Academic Press, New York, 1970), pp. 1–181.
[9] A. Georges, G. Kotliar, W. Krauth, and M. J. Rozenberg, Dynamical mean-field theory of strongly correlated Fermion

systems and the limit of infinite dimensions, Rev. Mod. Phys. **68**, 13 (1996).
[10] S. Y. Savrasov and G. Kotliar, Spectral density functionals for electronic structure calculations, Phys. Rev. B **69**, 245101 (2004).
[11] M. Gatti, V. Olevano, L. Reining, and I. V. Tokatly, Transforming nonlocality into a frequency dependence: A shortcut to spectroscopy, Phys. Rev. Lett. **99**, 057401 (2007).
[12] F. Aryasetiawan, L. Hedin, and K. Karlsson, Multiple plasmon satellites in Na and Al spectral functions from *ab initio* cumulant expansion, Phys. Rev. Lett. **77**, 2268 (1996).
[13] F. Caruso, C. Verdi, S. Poncé, and F. Giustino, Electron-plasmon and electron-phonon satellites in the angle-resolved photoelectron spectra of *n*-doped anatase TiO_2, Phys. Rev. B **97**, 165113 (2018).
[14] J. S. Zhou, L. Reining, A. Nicolaou, A. Bendounan, K. Ruotsalainen, M. Vanzini, J. J. Kas, J. J. Rehr, M. Muntwiler, V. N. Strocov *et al.*, Unraveling intrinsic correlation effects with angle-resolved photoemission spectroscopy, Proc. Natl. Acad. Sci. USA **117**, 28596 (2020).
[15] J. M. Luttinger and J. C. Ward, Ground-state energy of a many-fermion system. II, Phys. Rev. **118**, 1417 (1960).
[16] G. Baym and L. P. Kadanoff, Conservation laws and correlation functions, Phys. Rev. **124**, 287 (1961).
[17] G. Baym, Self-consistent approximations in many-body systems, Phys. Rev. **127**, 1391 (1962).
[18] R. M. Martin, L. Reining, and D. M. Ceperley, *Interacting Electrons: Theory and Computational Approaches* (Cambridge University Press, Cambridge, 2016).
[19] G. Stefanucci and R. V. Leeuwen, *Nonequilibrium Many-Body Theory of Quantum Systems: A Modern Introduction* (Cambridge University Press, Cambridge, 2013).
[20] C.-O. Almbladh, U. V. Barth, and R. V. Leeuwen, Variational total energies from ϕ- and ψ- derivable theories, Int. J. Mod. Phys. B **13**, 535 (1999).
[21] N. E. Dahlen and U. von Barth, Variational energy functionals tested on atoms, Phys. Rev. B **69**, 195102 (2004).
[22] K. Haule and G. L. Pascut, Forces for structural optimizations in correlated materials within a DFT+embedded DMFT functional approach, Phys. Rev. B **94**, 195146 (2016).
[23] T. Chiarotti, N. Marzari, and A. Ferretti, Unified Green's function approach for spectral and thermodynamic properties from algorithmic inversion of dynamical potentials, Phys. Rev. Res. **4**, 013242 (2022).
[24] B. Holm and U. von Barth, Fully self-consistent GW self-energy of the electron gas, Phys. Rev. B **57**, 2108 (1998).
[25] M. Puig von Friesen, C. Verdozzi, and C.-O. Almbladh, Kadanoff-Baym dynamics of Hubbard clusters: Performance of many-body schemes, correlation-induced damping and multiple steady and quasi-steady states, Phys. Rev. B **82**, 155108 (2010).
[26] S. Di Sabatino, P.-F. Loos, and P. Romaniello, Scrutinizing GW-based methods using the Hubbard dimer, Front. Chem. **9**, 751054 (2021).
[27] A. Honet, L. Henrard, and V. Meunier, Exact and many-body perturbation solutions of the Hubbard model applied to linear chains, AIP Adv. **12**, 035238 (2022).
[28] A. Kutepov, S. Y. Savrasov, and G. Kotliar, Ground-state properties of simple elements from GW calculations, Phys. Rev. B **80**, 041103(R) (2009).
[29] A. Kutepov, K. Haule, S. Y. Savrasov, and G. Kotliar, Electronic structure of Pu and Am metals by self-consistent relativistic *GW* method, Phys. Rev. B **85**, 155129 (2012).
[30] M. Grumet, P. Liu, M. Kaltak, J. C. V. Klimeš, and G. Kresse, Beyond the quasiparticle approximation: Fully self-consistent *GW* calculations, Phys. Rev. B **98**, 155143 (2018).
[31] C.-N. Yeh, S. Iskakov, D. Zgid, and E. Gull, Fully self-consistent finite-temperature *GW* in Gaussian Bloch orbitals for solids, Phys. Rev. B **106**, 235104 (2022).
[32] A. L. Kutepov and G. Kotliar, One-electron spectra and susceptibilities of the three-dimensional electron gas from self-consistent solutions of Hedin's equations, Phys. Rev. B **96**, 035108 (2017).
[33] K. Haule and T. Birol, Free energy from stationary implementation of the DFT + DMFT functional, Phys. Rev. Lett. **115**, 256402 (2015).
[34] C. P. Koçer, K. Haule, G. L. Pascut, and B. Monserrat, Efficient lattice dynamics calculations for correlated materials with DFT + DMFT, Phys. Rev. B **102**, 245104 (2020).
[35] S. L. Dudarev, G. A. Botton, S. Y. Savrasov, C. J. Humphreys, and A. P. Sutton, Electron-energy-loss spectra and the structural stability of nickel oxide: An LSDA + U study, Phys. Rev. B **57**, 1505 (1998).
[36] G. E. Engel, B. Farid, C. M. M. Nex, and N. H. March, Calculation of the GW self-energy in semiconducting crystals, Phys. Rev. B **44**, 13356 (1991).
[37] See Supplemental Material at http://link.aps.org/supplemental/10.1103/PhysRevResearch.6.L032023 for computational details and further discussions on the theoretical approach.
[38] S. Güttel and F. Tisseur, The nonlinear eigenvalue problem, Acta Numerica **26**, 1 (2017).
[39] Y. Su and Z. Bai, Solving rational eigenvalue problems via linearization, SIAM J. Matrix Anal. Appl. **32**, 201 (2011).
[40] Note that for simplicity of notation we dropped the identity on the *m*th bath, the correct Hamiltonian is $\Omega_m I_m$.
[41] S. Y. Savrasov, K. Haule, and G. Kotliar, Many-body electronic structure of americium metal, Phys. Rev. Lett. **96**, 036404 (2006).
[42] S. J. Bintrim and T. C. Berkelbach, Full-frequency GW without frequency, J. Chem. Phys. **154**, 041101 (2021).
[43] O. J. Backhouse, A. Santana-Bonilla, and G. H. Booth, Scalable and predictive spectra of correlated molecules with moment truncated iterated perturbation theory, J. Phys. Chem. Lett. **12**, 7650 (2021).
[44] S. J. Bintrim and T. C. Berkelbach, Full-frequency dynamical Bethe-Salpeter equation without frequency and a study of double excitations, J. Chem. Phys. **156**, 044114 (2022).
[45] C. J. C. Scott, O. J. Backhouse, and G. H. Booth, A "moment-conserving" reformulation of GW theory, J. Chem. Phys. **158**, 124102 (2023).
[46] A. Ferretti, T. Chiarotti, and N. Marzari, companion paper, Green's function embedding using sum-over-pole representations, Phys. Rev. B **110**, 045149 (2024).
[47] B. Himmetoglu, A. Floris, S. de Gironcoli, and M. Cococcioni, Hubbard-corrected DFT energy functionals: The LDA+U description of correlated systems, Int. J. Quantum Chem. **114**, 14 (2014).
[48] T. Miyake, C. Martins, R. Sakuma, and F. Aryasetiawan, Effects of momentum-dependent self-energy in the electronic

structure of correlated materials, Phys. Rev. B **87**, 115110 (2013).

[49] M. Vanzini and N. Marzari, Towards a minimal description of dynamical correlation in metals, arXiv:2309.12144.

[50] H. Jiang, R. I. Gomez-Abal, P. Rinke, and M. Scheffler, First-principles modeling of localized d states with the GW@LDA + U approach, Phys. Rev. B **82**, 045108 (2010).

[51] Explicitly, taking into account the periodicity of the crystal, the self-energy is: $\Sigma_{\rm dynH}(\omega) = \sum_{mm',\mathbf{R}} |\phi_{m,\mathbf{R}}\rangle \mathbf{\Sigma}^{mm',\mathbf{R}}_{\rm dynH}(\omega) \langle\phi_{m',\mathbf{R}}|$, with $|\phi_{m,\mathbf{R}}\rangle$ generic Wannier functions, and $\mathbf{\Sigma}^{mm',\mathbf{R}}_{\rm dynH}(\omega) = \langle\phi_{m,\mathbf{R}}|\Sigma_{\rm dynH}|\phi_{m',\mathbf{R}}\rangle$ independent of $\mathbf{R}$.

[52] The spectral function is calculated as $A(\omega) = \mathrm{sgn}(\mu - \omega)\mathrm{Im}G(\omega)$.

[53] M. Gatti and M. Guzzo, Dynamical screening in correlated metals: Spectral properties of $SrVO_3$ in the GW approximation and beyond, Phys. Rev. B **87**, 155147 (2013).

[54] L. Boehnke, F. Nilsson, F. Aryasetiawan, and P. Werner, When strong correlations become weak: Consistent merging of GW and DMFT, Phys. Rev. B **94**, 201106(R) (2016).

[55] S. Biermann, F. Aryasetiawan, and A. Georges, First-principles approach to the electronic structure of strongly correlated systems: Combining the GW approximation and dynamical mean-field theory, Phys. Rev. Lett. **90**, 086402 (2003).

[56] T. Ayral, S. Biermann, and P. Werner, Screening and nonlocal correlations in the extended Hubbard model from self-consistent combined GW and dynamical mean field theory, Phys. Rev. B **87**, 125149 (2013).

[57] J. P. Perdew, K. Burke, and M. Ernzerhof, Generalized gradient approximation made simple, Phys. Rev. Lett. **77**, 3865 (1996).

[58] J. P. Perdew, A. Ruzsinszky, G. I. Csonka, O. A. Vydrov, G. E. Scuseria, L. A. Constantin, X. Zhou, and K. Burke, Restoring the density-gradient expansion for exchange in solids and surfaces, Phys. Rev. Lett. **100**, 136406 (2008).

[59] J. M. Tomczak, M. Casula, T. Miyake, and S. Biermann, Asymmetry in band widening and quasiparticle lifetimes in $SrVO_3$: Competition between screened exchange and local correlations from combined GW and dynamical mean-field theory GW + DMFT, Phys. Rev. B **90**, 165138 (2014).

[60] R. Sakuma, P. Werner, and F. Aryasetiawan, Electronic structure of $SrVO_3$ within GW + DMFT, Phys. Rev. B **88**, 235110 (2013).

[61] T. Yoshida, K. Tanaka, H. Yagi, A. Ino, H. Eisaki, A. Fujimori, and Z.-X. Shen, Direct observation of the mass renormalization in $SrVO_3$ by angle resolved photoemission spectroscopy, Phys. Rev. Lett. **95**, 146404 (2005).

[62] M. Takizawa, M. Minohara, H. Kumigashira, D. Toyota, M. Oshima, H. Wadati, T. Yoshida, A. Fujimori, M. Lippmaa, M. Kawasaki, H. Koinuma, G. Sordi, and M. Rozenberg, Coherent and incoherent d band dispersions in $SrVO_3$, Phys. Rev. B **80**, 235104 (2009).

[63] T. Maekawa, K. Kurosaki, and S. Yamanaka, Physical properties of polycrystalline $SrVO_{3-\delta}$, J. Alloys Compd. **426**, 46 (2006).

[64] F. Birch, Finite elastic strain of cubic crystals, Phys. Rev. **71**, 809 (1947).

[65] T. Chiarotti, Spectral and thermodynamic properties of interacting electrons with dynamical functionals, Ph.D. thesis, École Polytechnique Fédérale de Lausanne, 2023.